Tuning of the Optoelectronic Properties for Transparent Oxide Semiconductor *A*SnO_3 by Modulating the Size of *A*-ions

Mian Wei[1]*, Hai Jun Cho[1,2], and Hiromichi Ohta[1,2]*

Keywords: transparent oxide semiconductor, $BaSnO_3$, $SrSnO_3$, $CaSnO_3$, optoelectronic properties, ionic radius, lattice parameter

ABSTRACT: Recently, La-doped *A*SnO_3 (*A* = Ba, Sr, and Ca) films have been attracted increasing attention as the active channel of deep-ultraviolet (DUV) transparent thin-film transistors (TFTs), owing to their wide bandgap and high electrical conductivity. However, the effect of *A*-site substitution on the optoelectronic properties of *A*SnO_3 has not been clarified in a detailed systematic study. Here we show that the optoelectronic properties of *A*SnO_3 can be tuned systematically by changing the average size of *A*-site ion. We heteroepitaxially fabricated *A*SnO_3 films on (001) $LaAlO_3$ substrates and measured their optical absorption spectra and electron transport properties. The lattice parameter almost linearly increased from 3.95 to 4.14 Å with increasing ionic radius of the *A*-site ion from 1.34 (Ca^{2+}) to 1.61 Å (Ba^{2+}), whereas the optical bandgap gradually decreased from ~4.6 to ~3.6 eV with a small positive bowing. With increasing the lattice parameter, the electrical conductivity gradually increased from ~10^0 to ~10^3 S cm^{-1} due to gradual

increases in both the carrier concentration and mobility. The present results are of significant importance for designing ASnO$_3$-based transparent electronic devices.

INTRODUCTION

Transparent oxide semiconductors (TOSs)[1-2], which transmit visible light, have been actively developed as the active layer of thin-film transistors (TFTs) for commercial flat panel displays such as liquid crystal displays and organic light emitting diodes.[3] Recently, expanding the transparency of TOSs to deep ultraviolet (DUV, 200−300 nm in wavelength) has become the key interest for developing the active material of next generation optoelectronics such as DUV sensors for biological applications.[4] However, conventional TOSs such as Sn-doped In_2O_3 (ITO, bandgap E_g ~3.5 eV)[5], amorphous $InGaZnO_4$ (E_g ~3 eV)[6] are opaque in DUV region due to their small bandgaps, whereas well-known DUV-TOSs such as β-Ga_2O_3 (E_g ~4.9 eV, ~1 S cm^{-1})[7-8], electron-doped calcium aluminate (C12A7:e^-, ~4 eV, ~800 S cm^{-1})[9-11], and Mg-substituted ZnO (~4.4 eV, ~1000 S cm^{-1})[12] show relatively low electron mobility, and the TFTs based on these materials exhibit poor performances.[13] The main challenge is balancing two conflicting physical properties: bandgap and electrical conductivity.

Recently, La-doped ASnO$_3$ (A = Ba, Sr, and Ca) films have attracted rising attention as the active TOS channel, owing to their wide bandgap and high electrical conductivity. La-doped $BaSnO_3$ (LBSO, E_g ~ 3.1 eV) thin films show high mobility values of 115−183 cm^2

V^{-1} s^{-1} at room temperature.[14-15] When a smaller Sr atom is substituted in the *A*-site, $SrSnO_3$ shows E_g of ~4.6 eV, allowing $SrSnO_3$-based TFT to transmit DUV light with a wavelength of 260 nm by more than 50%, which exhibit great potential in DNA-sensing in biology.[16] $ASnO_3$ has perovskite structure composed of corner-sharing SnO_6 octahedra. The crystal structure of $ASnO_3$ is closely related to lattice parameter, which determined by *A*-site substitution. Smaller *A*-site cations with stronger binding force increase atomic packing density and increase the interaction between atomic orbitals, which increases the splitting between the conduction band orbitals and valence band orbitals. This also triggers the deformations in the SnO_6 octahedral[17-18] and further induce structural phase transition in $ASnO_3$. Following this trend, if Ca, an even smaller alkaline element, occupies the *A*-site ($CaSnO_3$), further widening of the E_g value can be expected. However, the reported theoretical and experimental values of bandgap for $CaSnO_3$ are widely scattered from 1.95 to 5.38 eV.[19-21]

As shown in Figure 1, $BaSnO_3$ ($a = 4.116$ Å) is cubic crystal structure with the space group $Pm\bar{3}m$. $SrSnO_3$ ($a_{pc} = 4.037$ Å) and $CaSnO_3$ ($a_{pc} = 3.954$ Å) have a pseudo cubic crystal structure with the space group *Pnma*, distorted by a tilting in the SnO_6 octahedra. Thus, the lattice parameter of $ASnO_3$ can be modulated from 3.954 to 4.116 Å by substituting *A*-site. Although this system can potentially be an excellent solution for finding a good balance of optoelectronic properties, the effect of *A*-site substitution on the optoelectronic properties of $ASnO_3$ has not been clarified in detail due to the lack of

a systematic study.

Here we show that the optoelectronic properties of ASnO$_3$ in the solid solution systems. With increasing the average ionic radius of the *A*-site ion, the lattice parameter almost linearly increased from 3.95 to 4.14 Å while the optical bandgap decreased from ~4.6 to ~3.6 eV. With increasing the lattice parameter, the electrical conductivity gradually increased from ~10^0 to ~10^3 S cm^{-1} due to a gradual increase in both the carrier concentration and mobility. The electron transport properties of Ca-rich side solid solution films are greatly suppressed due to the large octahedral deformation, and La-CaSnO$_3$ showed an insulating behavior. On the other hand, La-SrSnO$_3$ exhibited a great balance of band gap and electrical performance, which makes it a suitable ASnO$_3$ system for advanced optoelectronic applications. The present results are of great value for designing ASnO$_3$ based transparent devices such as DUV-transparent TFTs.

RESULTS AND DISCUSSION

According to the XRD results, all resultant films were heteroepitaxially grown on (001) LaAlO$_3$ substrates while the RSM [Fig. 2(a)] of the resultant films were used to extract the lattice parameters perpendicular (*c*-axis) and parallel (*a*-axis) to the substrate surface. In order to directly compare the films, we used the average lattice parameter $(a \cdot c)^{1/3}$, which is plotted against the *A*-site ion substitution in Figure 2(b). Almost linear increase of lattice parameter was observed as a function of x in Ca$_{1-x}$Sr$_x$SnO$_3$, Sr$_{1-x}$Ba$_x$SnO$_3$, and

$Ba_{1-x}Ca_xSnO_3$, confirming that the ionic radius of the *A*-site ion can control the lattice parameter. We also calculated the lateral coherence length (*D*) of the *A*SnO_3 films [Fig. 2(c) and Table S1]. Although the average lattice parameters of the *A*SnO_3 films are different from each other, the *D* values are in the range of 20−30 nm, and there is no clear tendency against the lattice parameter.

Then, we measured the optical transmission [Fig. 3(a)] and reflection spectra of the resultant films and calculated the absorption coefficient α as $\alpha = -[\ln (T + R)] \cdot t^{-1}$, where *T*, *R*, and *t* are transmission, reflection, and thickness, respectively. The optical bandgap ($E_{g\ opt}$) was estimated from the $(\alpha h\nu)^2$–$h\nu$ plots [Fig. 3(b)]. Figure 3(c) and Table S2 show the $E_{g\ opt}$ of the resultant films as a function of average lattice parameter. The $E_{g\ opt}$ gradually decreased from 4.64 eV ($CaSnO_3$) to 3.59 eV ($BaSnO_3$) with increasing the lattice parameter. By adjusting the composition of solid solution, we can easily modulate the $E_{g\ opt}$ of *A*SnO_3. This is attributed to the interaction between O 2p and Sn 5s orbitals, which consist the valence band maximum (VBM) and conduction band minimum (CBM) of *A*SnO_3, respectively. The locations of the CBM and VBM are affected by the Sn–O bond length. When the distance between two adjacent Sn^{4+} and O^{2-} becomes shorter, the energy splitting between the antibonding state (=CBM) and bonding state (VBM) becomes greater. Therefore, the optical bandgap decreased with increasing the lattice parameter.

Figure 4 summarizes the room temperature electron transport properties [(a) electrical conductivity (σ), (b) carrier concentration (n), (c) Hall mobility (μ_{Hall}), (d) thermopower (S)] of the La-doped $Ca_{1-x}Sr_xSnO_3$, $Sr_{1-x}Ba_xSnO_3$, and $Ca_{1-x}Ba_xSnO_3$ solid solution films as a function of the average lattice parameter. The σ increases more than three orders of magnitude from ~0.5 to 2240 S cm^{-1} with increasing average lattice parameter, which is due to gradual increases in both n and μ_{Hall}. The observed n values are smaller than the nominal value, especially in the region of smaller lattice parameter. The absolute values of S gradually decrease with lattice parameter, which is consistent with the increase in n. The increasing tendency of n with lattice parameter is likely due to that the reduction of the bandgap. Suppression of μ_{Hall} fundamentally has two origins: increase in the carrier effective mass and reduction of relaxation time, where the latter strongly depends on the structural quality. For example, with the presence of boundaries, carrier transportation is suppressed at the boundary when the carrier concentration is low. According to the relationship between S and log n [Fig. S1],[22-23] the carrier effective mass of the films were in the range from 0.2 to 0.3 m_0, which cannot adequately explain the changes in μ_{Hall}. Therefore, we concluded that the A-site substitution does not significantly affect the carrier effective mass of the films. Thus, the small μ_{Hall} value at smaller lattice parameter side is mainly attributed to the reduction of relaxation time.

In order to further investigate the tendency of electron transport properties, we measured the temperature dependent electrical resistivity of the films [Fig. 5(a)]. In La-doped

$Ca_{1-x}Sr_xSnO_3$ and $Sr_{1-x}Ba_xSnO_3$ films, when lattice parameter is shorter than 3.97 Å, the ASnO$_3$ films showed insulating behavior. On the other hand, when the lattice parameter is greater than 4.01 Å, the films showed metallic behavior. The respective activation energy of the electrical conductivity (E_a) [Fig. 5(b), Table S3] gradually decreased from +22 to −14 meV with increasing the average lattice parameter. These results clearly indicate that the optoelectronic properties of ASnO$_3$ can be tuned by modulating the average *A*-site ionic radius.

These results indicate that larger *A*-site ion substitutions decrease the bandgap and the mobility edge. On the other hand, the carrier generation efficiency increases when the bandgap decreases. The carrier relaxation time increases when the mobility edge decreases. Thus, the electrical conductivity increases when a larger ion is substituted in the *A*-site. This systematic assessment will be of great value in designing ASnO$_3$ based transparent devices such as DUV-transparent TFTs.

CONCLUSION

In summary, we systematically investigated the optoelectronic properties of ASnO$_3$ epitaxial films on (001) LaAlO$_3$ substrates and demonstrated that ionic radius of *A*-site ion can be used to modulate the optoelectronic properties of ASnO$_3$. The lattice parameter can be controlled almost linearly from 3.95 to 4.14 Å with increasing the average ionic radius of the *A*-site ion from 1.34 (Ca^{2+}) to 1.61 Å (Ba^{2+}) while the optical bandgap

gradually decreased from ~4.6 to ~3.6 eV with a small positive bowing. The electrical conductivity gradually increased from ~10^0 to ~10^3 S cm^{-1} due to a gradual increase in both the carrier concentration and mobility according to the increase in the lattice parameter. The present results are of significantly importance for applying *A*SnO_3 in future transparent devices.

EXPERIMENTAL PROCEDURES

Epitaxial growth of the solid solution films: 3% La-doped solid solution epitaxial films were fabricated on (001) $LaAlO_3$ (a = 3.821 Å) single crystal substrates by pulsed laser deposition (PLD, KrF excimer laser, λ = 248 nm, fluence ~2 J cm^{-2} $pulse^{-1}$, repetition rate = 10 Hz). We used 3% La-doped *A*SnO_3 single phase ceramics as the PLD targets. During the film growth, the substrate temperature and oxygen pressure inside the chamber were kept at 750 °C and 20 Pa, respectively. In order to relax the lattice strain caused by the mismatch between film and substate, the thickness of all films was chosen to be ~200 nm.[24] Out-of-plane X-ray Bragg diffraction patterns of the solid solution thin films were measured by high-resolution X-ray diffraction (XRD, Cu $K\alpha_1$, ATX-G, Rigaku Co.) equipment. And the X-ray reflectivity spectra were also measured to evaluate the density and the thickness of films. The X-ray reciprocal space mappings (RSMs) were recorded to clarify the change of the lateral (in-plane) coherence lendgth (D) evaluated from the diffraction spots using Scherrer equation. Detailed structural characterizations are described elsewhere.[24-26]

Optoelectronic property measurements: A spectrophotometer (solidspec-3700, Shimazu Co.) was used to collect ultraviolet-visible (UV-vis) diffuse reflectance data in 200−1700 nm wavelength range. The optical bandgap ($E_{g\ opt}$) was calculated using the Tauc plot, $(\alpha hv)^2 = C\ (hv - E_g)$. The electrical conductivity (σ), carrier concentration (n), and Hall mobility (μ_{Hall}) of the films were measured in the in-plane direction using the conventional dc four-probe method with van der Pauw electrode configuration. The thermopower (S) was acquired from the thermos-electromotive force (ΔV) generated by a temperature difference (ΔT) of ~4 K across the film using two Peltier devices. The temperatures at each end of the films were simultaneously measured with two thermocouples, and the S-values were calculated from the slope of the ΔT−ΔV plots (correlation coefficient: > 0.9999).

ASSOCIATED CONTENT

Supporting Information

The Supporting Information is available free of charge via the Internet at https://pubs.acs.org.

Thermopower (−S) of the resultant films as a function of carrier concentration (n) at room temperature. Optical transmission spectra of the ASnO$_3$ films (film thickness: 100nm). Crystallographic analyses of the La-doped ASnO$_3$ solid solution films. Optical

transmission in wavelength of 260 nm and bandgap of the *A*SnO_3 solid solution films. Activation energy of the electrical conductivity for the La-doped *A*SnO_3 solid solution films.

AUTHOR INFORMATION

Corresponding Authors

Mian Wei

Graduate School of Information Science and Technology, Hokkaido University, N14W9, Kita, Sapporo 060−0814, Japan

ORCiD: orcid.org/0000-0001-9793-4325

Email: wm3256@gmail.com

Hiromichi Ohta

Research Institute for Electronic Science, Hokkaido University, N20W10, Kita, Sapporo 001-0020, Japan

ORCiD: orcid.org/0000-0001-7013-0343

Email: hiromichi.ohta@es.hokudai.ac.jp

Authors

Hai Jun Cho

Research Institute for Electronic Science, Hokkaido University, N20W10, Kita, Sapporo 001-0020, Japan

ORCiD: orcid.org/0000-0002-8642-4183

Author Contributions

M.W. performed the sample preparation and measurements. H.O. planned and supervised the project. All authors discussed the results and commented on the manuscript.

Funding Sources

Mian Wei received scholarship from the China Scholarship Council (201808050081). Hai Jun Cho received funding from Nippon Sheet Glass Foundation for Materials Science and Engineering. Hiromichi Ohta received founding from Grants-in-Aid of the JSPS (19H05791 and 17H01314).

Notes

The authors declare no competing financial interest.

ACKNOWLEDGMENTS

This research was supported by Grants-in-Aid for Scientific Research A (17H01314) and Innovative Areas (19H05791) from the JSPS. H.J.C. acknowledges the support from Nippon Sheet Glass Foundation for Materials Science and Engineering. The support from

China Scholarships Council (M. Wei: 201808050081) is also greatly appreciated. A part of this work was supported by Dynamic Alliance for Open Innovation Bridging Human, Environment, and Materials, and by the Network Joint Research Center for Materials and Devices.

REFERENCES

(1) Ginley, D.; Hosono, H.; Paine, D. C., *Handbook of Transparent Conductors*. 2011th Edition ed.; Springer: 2011.

(2) Hosono, H., Recent progress in transparent oxide semiconductors: Materials and device application. *Thin Solid Films* **2007,** *515*, 6000-6014.

(3) Hosono, H., How We Made the IGZO Transistor. *Nat. Electron.* **2018,** *1*, 428-428.

(4) Kim, J.; Campbell, A. S.; de Avila, B. E. F.; Wang, J., Wearable biosensors for healthcare monitoring. *Nat. Biotechnol.* **2019,** *37*, 389-406.

(5) Kerkache, L.; Layadi, A.; Dogheche, E.; Remiens, D., Physical properties of RF sputtered ITO thin films and annealing effect. *J. Phys. D: Appl. Phys.* **2005,** *39*, 184.

(6) Orita, M.; Ohta, H.; Hirano, M.; Narushima, S.; Hosono, H., Amorphous transparent conductive oxide $InGaO_3(ZnO)_m$ ($m \leq 4$): a Zn 4s conductor. *Philos. Mag. B* **2001,** *81*, 501-515.

(7) Orita, M.; Ohta, H.; Hirano, M.; Hosono, H., Deep-ultraviolet transparent conductive beta-Ga_2O_3 thin films. *Appl. Phys. Lett.* **2000,** *77*, 4166-4168.

(8) Wakabayashi, R.; Yoshimatsu, K.; Hattori, M.; Ohtomo, A., Epitaxial structure and electronic property of beta-Ga_2O_3 films grown on MgO (100) substrates by pulsed-laser deposition. *Appl. Phys. Lett.* **2017,** *111*, 162101.

(9) Miyakawa, M.; Hayashi, K.; Hirano, M.; Toda, Y.; Kamiya, T.; Hosono, H., Fabrication of highly conductive $12CaO\text{-}7Al_2O_3$ thin films encaging hydride ions by proton implantation. *Adv. Mater.* **2003,** *15*, 1100.

(10) Matsuishi, S.; Toda, Y.; Miyakawa, M.; Hayashi, K.; Kamiya, T.; Hirano, M.; Tanaka, I.; Hosono, H., High-density electron anions in a nanoporous single crystal:

$Ca_{24}Al_{28}O_{64}^{4+}4e^-$. *Science* **2003,** *301*, 626-629.

(11) Hayashi, K.; Matsuishi, S.; Kamiya, T.; Hirano, M.; Hosono, H., Light-induced conversion of an insulating refractory oxide into a persistent electronic conductor. *Nature* **2002,** *419*, 462-465.

(12) Segura, A.; Sans, J. A.; Errandonea, D.; Martinez-Garcia, D.; Fages, V., High conductivity of Ga-doped rock-salt ZnO under pressure: Hint on deep-ultraviolet-transparent conducting oxides. *Applied Physics Letters* **2006,** *88*, 011910.

(13) Matsuzaki, K.; Yanagi, H.; Kamiya, T.; Hiramatsu, H.; Nomura, K.; Hirano, M.; Hosono, H., Field-induced current modulation in epitaxial film of deep-ultraviolet transparent oxide semiconductor Ga_2O_3. *Appl. Phys. Lett.* **2006,** *88*, 092106.

(14) Paik, H.; Chen, Z.; Lochocki, E.; Seidner H, A.; Verma, A.; Tanen, N.; Park, J.; Uchida, M.; Shang, S.; Zhou, B.-C.; Brützam, M.; Uecker, R.; Liu, Z.-K.; Jena, D.; Shen, K. M.; Muller, D. A.; Schlom, D. G., Adsorption-controlled growth of La-doped $BaSnO_3$ by molecular-beam epitaxy. *APL Mater.* **2017,** *5*, 116107.

(15) Sanchela, A.; Wei, M.; Lee, J.; Kim, G.; Jeen, H.; Feng, B.; Ikuhara, Y.; Cho, H. J.; Ohta, H., Buffer layer-less fabrication of a high-mobility transparent oxide semiconductor, La-doped $BaSnO_3$. *J. Mater. Chem. C* **2019,** *7*, 6.

(16) Wei, M.; Sanchela, A. V.; Feng, B.; Ikuhara, Y.; Cho, H. J.; Ohta, H., High electrical conducting deep-ultraviolet-transparent oxide semiconductor La-doped $SrSnO_3$ exceeding similar to 3000 S cm^{-1}. *Appl. Phys. Lett.* **2020,** *116*, 022103.

(17) Cho, H. J.; Sato, K.; Wei, M.; Kim, G.; Ohta, H., Effect of lattice distortions on the electron and thermal transport properties of transparent oxide semiconductor $Ba_{1-x}Sr_xSnO_3$ solid solution films. *J. Appl. Phys.* **2020,** *127*, 115701.

(18) Mountstevens, E. H.; Attfield, J. P.; Redfern, S. A., Cation-size control of

structural phase transitions in tin perovskites. *J. Phys.: Condens. Matter* **2003,** *15*, 8315.

(19) Henriques, J. M.; Caetano, E. W. S.; Freire, V. N.; da Costa, J. A. P.; Albuquerque, E. L., Structural, electronic, and optical absorption properties of orthorhombic $CaSnO_3$ through *ab* initio calculations. *J. Phys.-Condens. Matter* **2007,** *19*, 106214.

(20) Zhang, W. F.; Tang, J. W.; Ye, J. H., Structural, photocatalytic, and photophysical properties of perovskite $MSnO_3$ (*M* = Ca, Sr, and Ba) photocatalysts. *J. Mater. Res.* **2007,** *22*, 1859-1871.

(21) Liu, Q. Z.; Jin, F.; Li, B.; Geng, L., Structure and band gap energy of $CaSnO_3$ epitaxial films on $LaAlO_3$ substrate. *J. Alloy. Compd.* **2017,** *717*, 55-61.

(22) Sanchela, A. V.; Wei, M.; Cho, H. J.; Ohta, H., Thermopower Modulation Clarification of the Operating Mechanism in Wide Bandgap $BaSnO_3$-$SrSnO_3$ Solid-Solution Based Thin Film Transistors. *Small* **2019,** *15*, 1805394.

(23) Sanchela, A.; Onozato, T.; Feng, B.; Ikuhara, Y.; Ohta, H., Thermopower modulation clarification of the intrinsic effective mass in transparent oxide semiconductor $BaSnO_3$. *Phys. Rev. Mater.* **2017,** *1*, 5.

(24) Sanchela, A. V.; Wei, M.; Zensyo, H.; Feng, B.; Lee, J.; Kim, G.; Jeen, H.; Ikuhara, Y.; Ohta, H., Large thickness dependence of the carrier mobility in a transparent oxide semiconductor, La-doped $BaSnO_3$. *Appl. Phys. Lett.* **2018,** *112*, 232102.

(25) Cho, H. J.; Onozato, T.; Wei, M.; Sanchela, A.; Ohta, H., Effects of vacuum annealing on the electron mobility of epitaxial La-doped $BaSnO_3$ films. *APL Mater.* **2019,** *7*, 022507.

(26) Sanchela, A.; Wei, M.; Lee, J.; Kim, G.; Jeen, H.; Feng, B.; Ikuhara, Y.; Cho, H. J.; Ohta, H., Buffer layer-less fabrication of high-mobility transparent oxide

semiconductor, La-doped $BaSnO_3$. *J. Mater. Chem. C* **2019,** *7*, 5797.

(27) Shannon, R. D., Revised Effective Ionic-Radii and Systematic Studies of Interatomic Distances in Halides and Chalcogenides. *Acta Crystallogr. A* **1976,** *32*, 751-767.

Table 1. Electrical and optical properties of the La-doped ASnO$_3$ (A = Ca, Sr, Ba) films.

A-site ion	n (10^{19} cm^{-3})	μ_{Hall} (cm^2 V^{-1} s^{-1})	σ (S cm^{-1})	E_g (eV)
Ca^{2+}	–	–	–	4.64
Sr^{2+}	23	51	1900	4.43
Ba^{2+}	22	64	2235	3.59

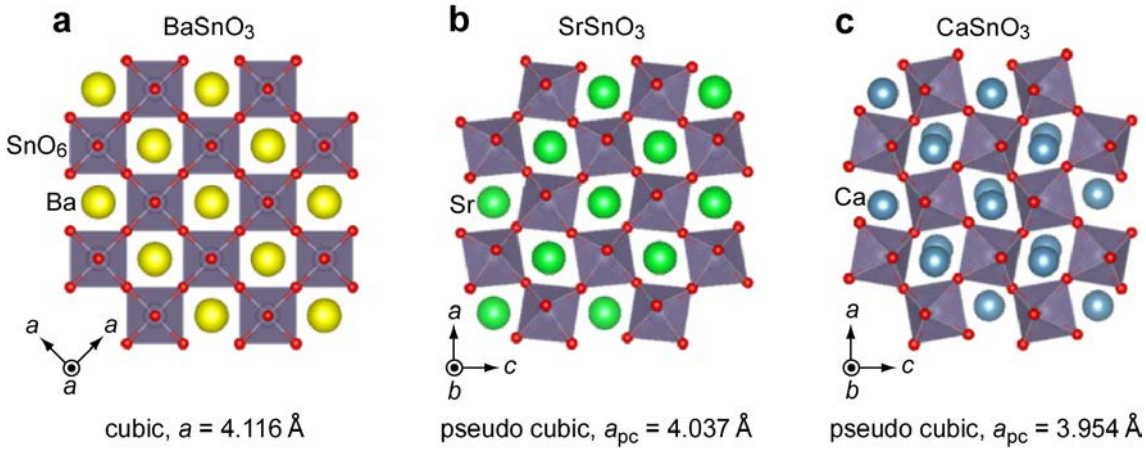

Figure 1. Schematic crystal structure of (a) $BaSnO_3$ (b) $SrSnO_3$ and (c) $CaSnO_3$. Crystal structures were obtained from the Rietveld refinement of the powder XRD patterns. $ASnO_3$ (*A* = Ca, Sr, Ba) consisting of layers of SnO_6 octahedra separated by *A* atoms. $BaSnO_3$ (a = 4.116 Å) is cubic crystal structure with the space group *Pm*-3*m*, $SrSnO_3$ (a_{pc} = 4.037 Å) and $CaSnO_3$ (a_{pc} = 3.954 Å) are orthorhombic crystal structure with the space group *Pnma*. The Shannon's ionic radius of Ca^{2+} is 1.34 Å, Sr^{2+} is 1.44 Å, and Ba^{2+} is 1.61 Å, respectively, when the coordination number is 12.[27]

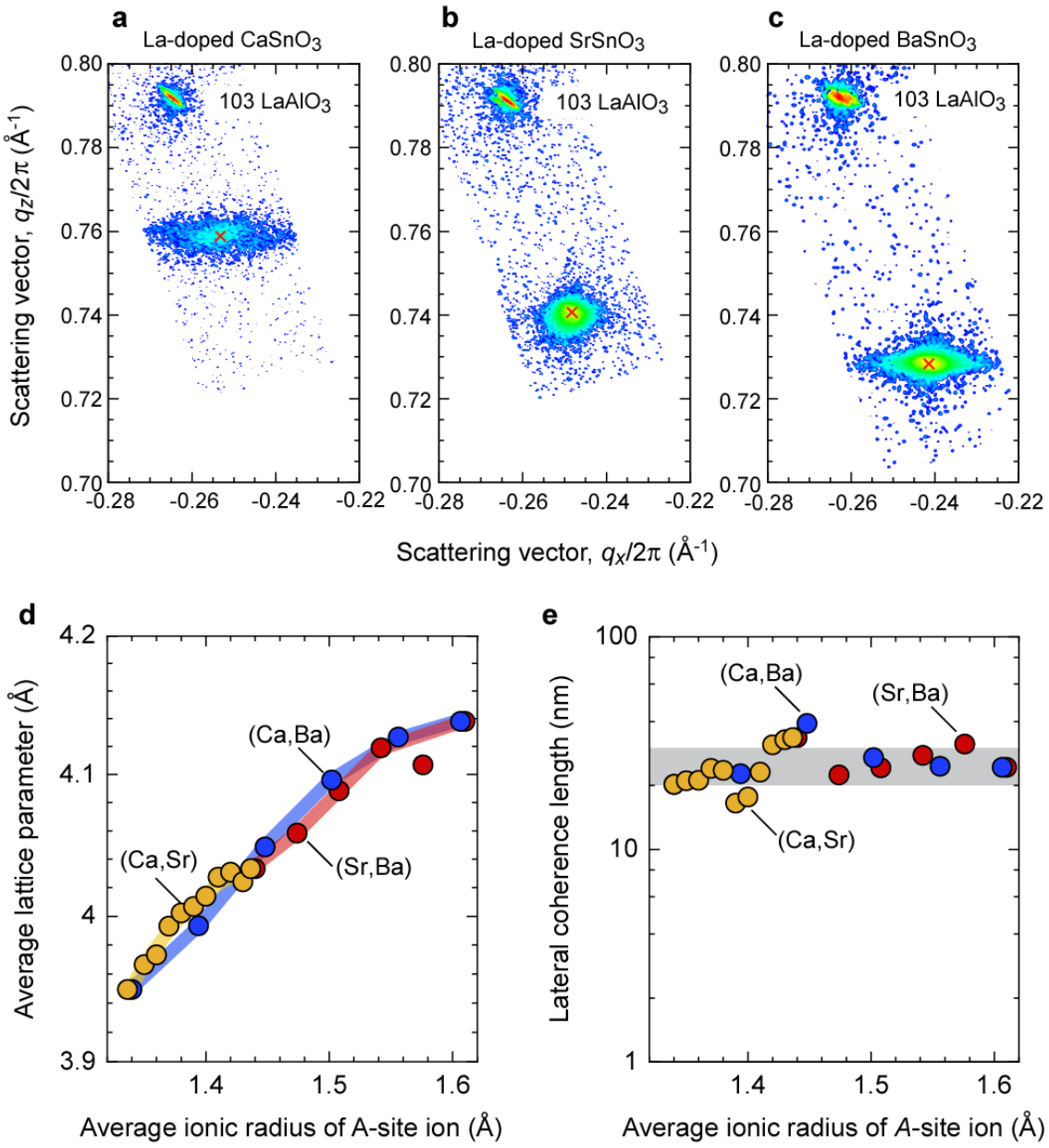

Figure 2. Crystallographic analyses of the ASnO$_3$ films grown on (001) LaAlO$_3$ substrates. (a–c) Reciprocal space mappings of (a) CaSnO$_3$, (b) SrSnO$_3$, and (c) BaSnO$_3$. Red x indicates the peak position of the diffraction spot of 103 ASnO$_3$. (d) Relationship between average lattice parameter and average ionic radius of A-site ion in ASnO$_3$. Solid line indicates the fitted curve. (e) Lateral coherence length of the ASnO$_3$ films plotted as a function of average ionic radius of A-site ion. The lateral coherence length is ranging 20–30 nm and independent on the average ionic radius.

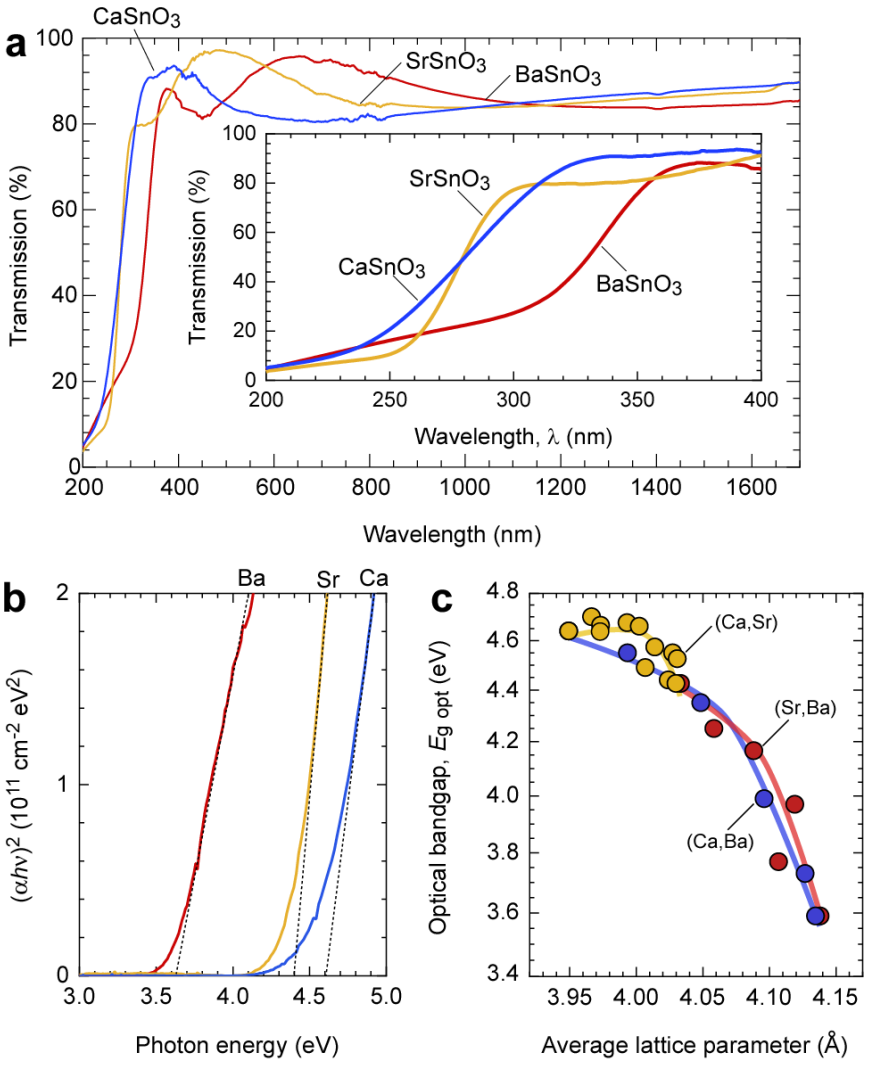

Figure 3. Optical properties of the ASnO$_3$ films. (a) Optical transmission spectra of the ASnO$_3$ films. The film thickness was ~100 nm. The inset shows the magnified spectra around DUV region. (b) $(\alpha h\upsilon)^2$–$h\upsilon$ plots. (c) Optical bandgap ($E_{g\ opt}$) plotted as a function of average lattice parameter. $E_{g\ opt}$ gradually decreases with increasing lattice parameter. The $E_{g\ opt}$ of the CaSnO$_3$, SrSnO$_3$, and BaSnO$_3$ films are 4.64, 4.43, and 3.59 eV, respectively.

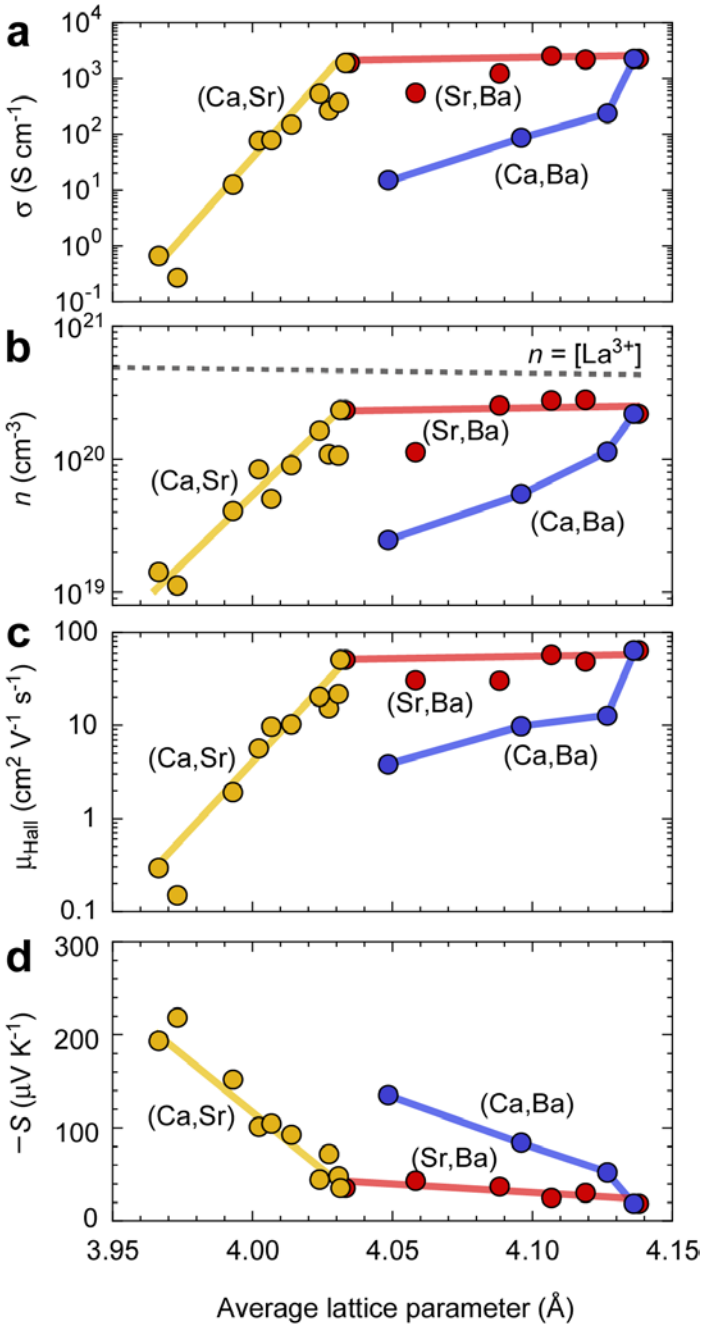

Figure 4. Room temperature electron transport properties of the La-doped $Ca_{1-x}Sr_xSnO_3$, $Sr_{1-x}Ba_xSnO_3$ and $Ca_{1-x}Ba_xSnO_3$ solid solution films as a function of average lattice parameter. (a) electrical conductivity (σ), (b) carrier concentration (n), (c) Hall mobility (μ_{Hall}), (d) thermopower (S). The solid lines are guide for the eyes. The dotted line in (a) indicates n when doped La is fully activated. Both n and μ_{Hall} gradually increase with increasing the lattice parameter and, therefore, σ increases with lattice parameter. The increasing tendency of n is confirmed by the decreasing tendency of $-S$.

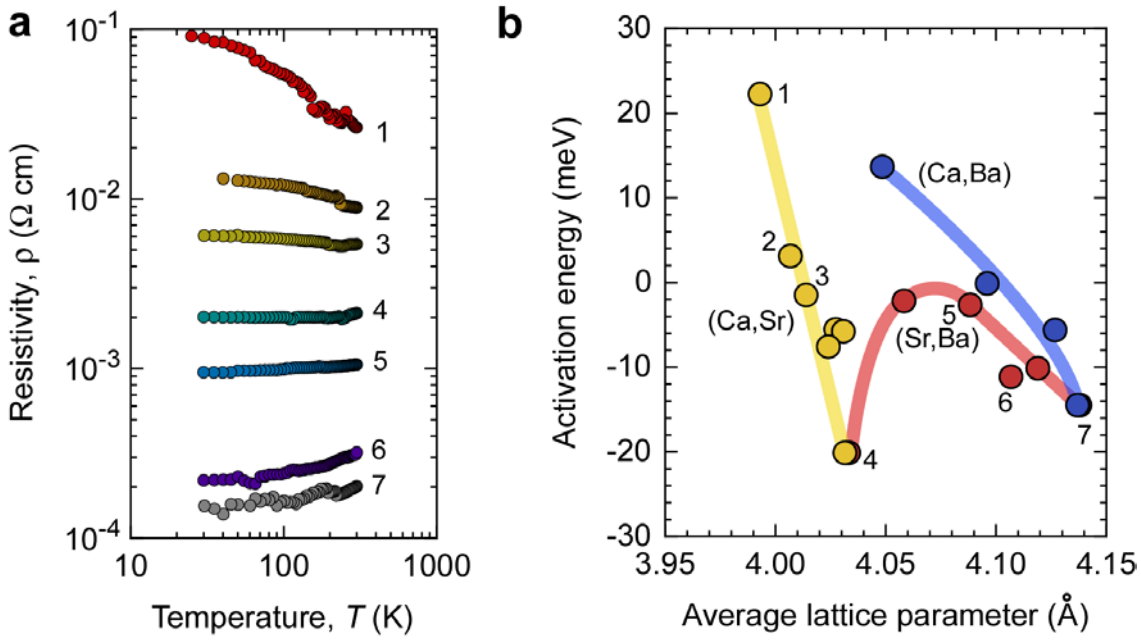

Figure 5. Activation energy of the electrical conductivity. (a) Temperature dependence of the electrical resistivity of the ASnO$_3$ films with various lattice parameters. (b) Activation energy of the electrical conductivity (E_a), which was calculated using the Arrhenius plot.

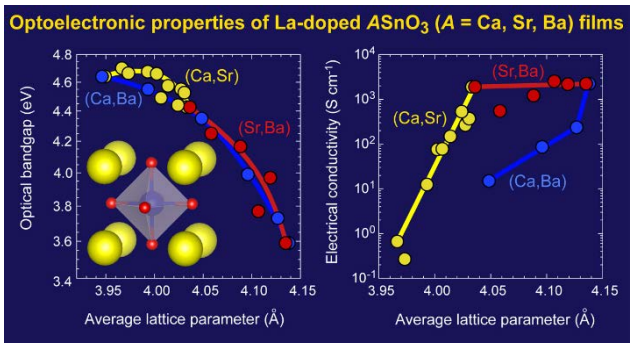
Optoelectronic properties of La-doped ASnO3 (A = Ca, Sr, Ba) films
Optical bandgap (eV)
4.8
4.6
4.4
4.2
4.0
3.8
3.6
3.4
(Ca,Sr)
(Ca,Ba)
(Sr,Ba)
3.95
4.00
4.05
4.10
4.15
Average lattice parameter (Å)
Electrical conductivity (S cm-1)
10^4
10^3
10^2
10^1
10^0
10^-1
(Sr,Ba)
(Ca,Sr)
(Ca,Ba)
3.95
4.00
4.05
4.10
4.15
Average lattice parameter (Å)